(Received 5 November 2024, Accepted 6 December 2024, Scheduled 13 December 2024)

A Bandpass Filter Using Substrate Integrated Waveguide Cavity for Nonlinear Junction Detection Applications

Boyan Zhang, Minquan Li*, Guocui Zhu, Yongkang Yuan, Chen Li, Shuang Xiao, and Xin Qu

Anhui University, China

ABSTRACT: A band-pass filter utilizing a dual-mode Substrate Integrated Waveguide (SIW) cavity, enhanced by a novel Defected Ground Structure (DGS) is proposed in this paper. The SIW cavity operates in TE_{110} and TE_{120} modes, and the electric field of TE_{110} is modified by introducing a series of metallized disturbance holes at the center of SIW cavity to increase the resonant frequency of TE_{110} mode to that of TE_{120} mode, thereby forming a passband with two transmission poles. A DGS that combines a dumbbell structure with a Complementary Split Ring Resonator (CSRR) is employed on the ground plane of the filter to improve the stopband rejection and suppress the parasitic passband. EM simulation and measurement results suggest that the center frequency of the filter is 4.8 GHz. It achieves a 3 dB-bandwidth of 300 MHz, with its insertion loss in the passband up to 0.5 dB and return loss greater than 20 dB. The designed DGS introduces a transmission zero near 7.2 GHz to suppress the parasitic passband and enhance the selectivity of the filter, while maintaining the original insertion loss and return loss within the passband. Its overall layout is simple and innovative. The designed filter is specifically engineered for application in the receiver of Nonlinear Junction Detection (NLJD) systems, aiming to suppress interference signals and allow only the second harmonic to pass through, which holds certain practical significance in RF engineering.

1. INTRODUCTION

With the swift advancement of wireless communication systems and microwave passive devices, microwave filters featuring high performance, high efficiency, and miniaturization have drawn increasing attention. In Radio Frequency (RF) transceiver systems, radar systems, 5G communications, and other domains, microwave filters play an irreplaceable role in frequency selection and interference suppression. Consequently, the exploration regarding the performance enhancement and structural innovation of microwave filters has emerged as a popular subject in recent years [1–3].

As a novel planar structure, Substrate Integrated Waveguide (SIW) has been extensively adopted in the design of microwave filters and microwave circuit systems in recent years. In comparison with microstrip structure, SIW has the advantages of low insertion loss, ease of integration, and strong anti-interference capability [4–7]. Meanwhile, as a novel approach in the design of microwave passive devices, Defected Ground Structure (DGS) has been commonly employed to enhance stopband suppression, eliminate parasitic passbands, and inhibit higher-order modes [8–11]. At the same time, with the development of sub-wavelength artificial materials, metamaterials which can realize electromagnetic properties that do not exist in nature, such as negative permittivity and negative permeability, are constantly being applied to the design of microwave filters [12–15].

Over the recent years, a considerable number of high-performance microwave filter designs have utilized SIW and DGS technology [16–19]. Ref. [16] presents a SIW filter with mushroom-shaped metallized resonators, generating a quasi-elliptic response and four transmission poles in the passband. The resonant frequency is controlled by adjusting the distance of stalk shift and stalk diameter; however, the parasitic passband is close, and the insertion loss in the passband has room for improvement. Ref. [17] introduces a series of quarter-mode SIW cavity filters, considering side coupling and corner coupling to achieve high-performance and compact filters, but the out-of-band rejection performance requires enhancement, and the parasitic passband is close. Ref. [18] provides an in-line port-fed SIW filter with a dual-mode response, applying metallized perturbation holes near the SIW cavity to separate uncoupled modes TE_{102} and TE_{201}. Thus, a passband with two transmission poles is formed, and the transmission zeros are adjusted by changing the position of the perturbation holes. Three types of filters are designed based on this principle, but their stopband performance is unsatisfactory. In [19], a SIW filter using a mixed coupling technique to enhance selectivity is proposed to generate transmission zeros without compromising the advantages of SIW. The filter produces a flat passband with excellent return loss and insertion loss performance, while its out-of-band rejection is outstanding, and the parasitic passband is distant.

In previous studies, many SIW band-pass filters were designed by disrupting the resonant mode in the cavity and adding multiple DGSs to form a passband. From the results of simulation and measurement, it can be seen that these filters generally have close parasitic passband or unsatisfactory stopband suppression. For these filters, the introduction of DGS typically resolves these problems. However, such introduction usually leads to the degradation of the performance regarding in-band

* Corresponding author: Minquan Li (AHU411MHz@hotmail.com).

insertion loss and return loss, thereby causing the SIW structure to partially lose its original advantages. In order to solve the problem above, a microwave band-pass filter based on SIW is designed in this paper, in combination with the application requirements of the receiver module of the Nonlinear Junction Detection (NLJD) system to receive and process the second harmonic signal reflected by the nonlinear node [20]. The proposed filter operates in TE_{110} and TE_{120} modes, and the electric field of TE_{110} mode is disturbed to increase its resonant frequency to that of TE_{120} to form the desired passband. The DGS adopted in this paper enhances the selectivity of the filter, suppresses the parasitic passband, and has negligible effect on the insertion loss and return loss within the passband, whose layout is both simple and innovative. Simulated and experimental results indicate that the filter proposed in this paper exhibits excellent performance in desired frequency selection and parasitic passband suppression. The designed filter is specifically engineered for application in the receiver of NLJD systems, aiming to suppress interference signals and allow only the second harmonic to pass through.

The contents of each section in this paper are as follows. Section 1 gives the background of the proposed filter. Section 2 introduces the structure and layout of the proposed filter. Section 3 introduces the working principle of each filter structure. In Section 4, Electromagnetic (EM) simulation results, measured results, and correlated analysis are given. Section 5 gives the conclusion of the paper.

2. FILTER STRUCTURE

The proposed filter adopts a single-layer SIW structure, and its 3D geometrical structure is presented in Fig. 1. The filter is composed of metal layers on both the top and bottom sides of the dielectric plate. Meanwhile, the thickness of the dielectric plate and both metal layers are 1 mm and 35 µm, respectively. The substrate material is Taconic TLY-5, with a relative permittivity of $\varepsilon_r = 2.2$ and a loss tangent of $\tan\delta = 0.0009$. In this design, the shape of the SIW cavity assumes a rectangular form, and the primary transmission modes of the EM wave are TE_{110} and TE_{120}. A series of metallized via-holes are positioned along the x-axis direction at the center of the proposed SIW cavity to disturb the electric field of the TE_{110} mode, thereby enabling the resonant frequency of the TE_{110} mode to be closer to that of the TE_{120} mode. The input and output ports of the proposed filter are fed by microstrip lines with a characteristic impedance of 50 Ω. Meanwhile, the impedance matching from the microstrip to the SIW cavity is achieved through coplanar waveguide transition and is adjusted by the penetration depth of the feedline into the cavity. A DGS is etched on the bottom metal layer of the proposed filter, which adopts a combination of a dumbbell structure and a Complementary Spilt Ring Resonator (CSRR), in order to introduce a transmission zero into the high-frequency area and thereby enhance the stopband rejection of the filter. The layout of each layer is shown in Fig. 2, and the dimensional parameters after optimization using High Frequency Structure Simulator (HFSS) are shown in Table 1.

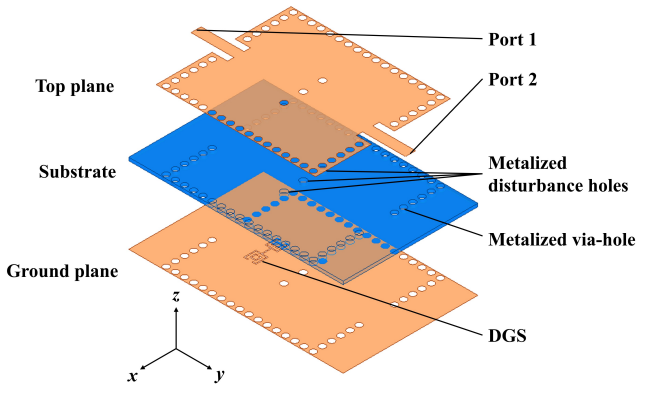

FIGURE 1. The composition of the proposed filter.

TABLE 1. Geometrical dimensions of the proposed filter (Units: mm).

d	L	L_1	s	s_1	W	W_1	g_t
2	48	14	3	6.3	41.5	3.3	2.1
s_2	g	g_i	g_o	L_d	L_o	W_d	
12	0.7	0.5	1.4	3	4	0.3	

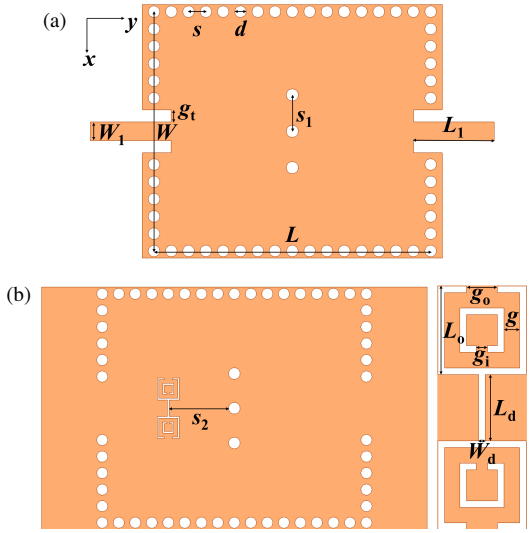

FIGURE 2. Geometrical layout of each layer. (a) Top layer; (b) Ground layer with DGS structure.

3. WORKING PRINCIPLE OF THE DESIGNED FILTER

The Substrate Integrated Waveguide (SIW) has evolved from the conventional dielectric-filled rectangular waveguide. By substituting the metal walls on both sides of the rectangular waveguide with metallized through-holes, the SIW is formed. In this manner, a planar transmission line structure with waveguide characteristics can be achieved on a Printed Circuit Board (PCB). As a novel waveguide-like structure, the EM wave transmission characteristic of the SIW is nearly the same as that of the rectangular waveguide. Since the periodic metallized via-holes at the edge of the SIW cavity cut off the surface current along the x-axis, the SIW cavity is unable to transmit EM waves in TM mode and can only be used for transmitting

TE mode. The resonant frequency $f_{\mathrm{TE}_{mn0}}$ corresponding to the TE_{mn0} mode is determined by the geometrical parameters of the SIW cavity, which is

$$f_{\mathrm{TE}_{mn0}} = \frac{c}{2\sqrt{\varepsilon_r}} \cdot \sqrt{\left(\frac{m}{W_{eff}}\right)^2 + \left(\frac{n}{L_{eff}}\right)^2} \tag{1}$$

In Equation (1), c represents the speed of light; ε_r denotes the relative dielectric constant of the substrate; m and n respectively stand for the number of nodal points along the x and y-axis, while W_{eff} and L_{eff} respectively signify the effective width and length of the SIW cavity. The effective width and length are determined by the physical dimensions of SIW cavity [3]

$$W_{eff} = W + \frac{d^2}{0.95s} \tag{2}$$

$$L_{eff} = L + \frac{d^2}{0.95s} \tag{3}$$

In Equations (2) and (3), parameters L and W denote the physical length of the proposed SIW cavity, while d stands for the diameter of cylindrical metallized via-holes, and s represents the distance between the adjacent holes. During the process of designing the SIW cavity, the parameters of the through-hole diameter d and spacing s are of great significance. This is because these two parameters will directly determine the radiation loss of the SIW cavity. Excessive radiation loss will undoubtedly lead to a severe degradation of the passband performance of the SIW filter. To minimize the radiation loss, parameters d and s should satisfy the following inequalities

$$s \leq 2d \quad \text{and} \quad d < \frac{\lambda_g}{5} \tag{4}$$

where λ_g represents the waveguide wavelength in SIW [3]. Subsequently, the SIW cavity filter can be designed by employing the method of analyzing conventional rectangular waveguide.

The proposed band-pass filter is designed to operate at the frequency of the second harmonic. Since the NLJD transmitter is configured to transmit at 2.4 GHz, the center frequency of the proposed filter is set at 4.8 GHz, which will also be the resonant frequency of the TE_{120} mode. Based on the Equations (1), (2) and (3), the size of the proposed SIW cavity is anticipated to be $L = 48$ mm and $W = 41.5$ mm. EM simulation was performed on the SIW cavity (whose structure is presented in Fig. 3) of determined size. The S-parameter plot

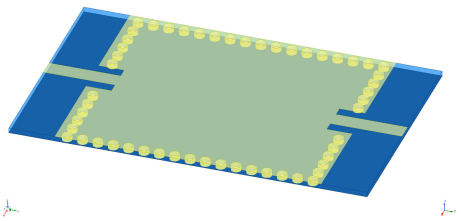

FIGURE 3. Structure of the designed SIW cavity.

and E-field distribution at different frequencies are respectively presented in Fig. 4 and Fig. 5. The S-parameter plot indicates that the designed SIW cavity resonates at 3.25 GHz, 4.8 GHz, 6.72 GHz, and 7.88 GHz, while the E-field distribution reveals that the transmission modes at these frequencies are TE_{110}, TE_{120}, TE_{130}, and TE_{310}, respectively.

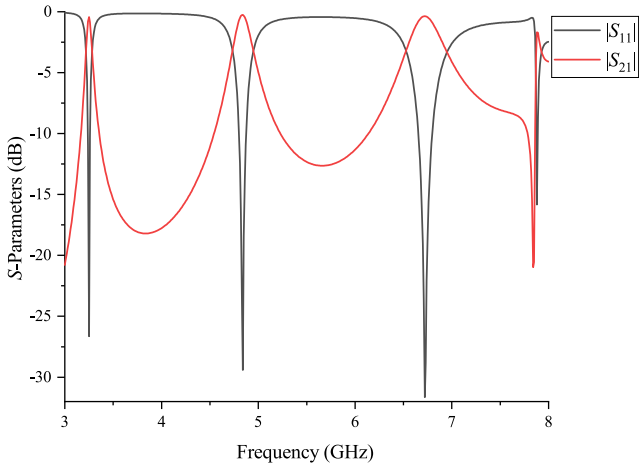

FIGURE 4. Simulated S-parameter of the designed SIW cavity.

To form a passband at the desired frequency, three metallized via-holes are uniformly positioned at the center of the SIW cavity along the x-axis direction to perturb the electric field of the TE_{110} mode. In this manner, the equivalent cavity size of TE_{110} mode is reduced, and its resonant frequency shifts towards the high-frequency direction. Since these perturbation holes are placed in the region where the electric field intensity of TE_{120} mode is minimal, the influence of these holes on the TE_{120} mode is limited, thus its resonant frequency will not be changed. It is noteworthy that the perturbation holes also have an impact on the electric fields of the TE_{130} and TE_{310} modes, and similarly, the resonant frequencies of these two modes shift towards the direction of higher frequencies.

The structure and EM simulation of the SIW cavity with disturbance holes (referred to as BPF_1 hereinafter) are conducted in Fig. 6 and Fig. 7, respectively. It can be observed that the BPF_1 forms a passband at 4.8 GHz. The return loss within the passband is greater than 24.02 dB, and the insertion loss amounts to 0.30 dB. There are two transmission poles in the passband, corresponding to TE_{110} and TE_{120} modes, respectively. The E-field distribution of BPF_1 at different frequencies is shown in Fig. 8. Fig. 8 indicates that TE_{110} and TE_{120} modes have a higher electric field intensity at the input and output ports; therefore, these two modes can be excited in the cavity. However, the high-order mode TE_{220} can also be transmitted in the cavity, which causes the filter to generate a parasitic passband at 7.78 GHz. The parasitic passband should be suppressed appropriately; otherwise, it will affect the selectivity and stopband attenuation performance of the filter.

To address the issue of performance deterioration resulting from the parasitic passband, DGS is incorporated into the designed filter. DGS alters the transmission characteristics of microwave circuits by etching a specific shape on the ground

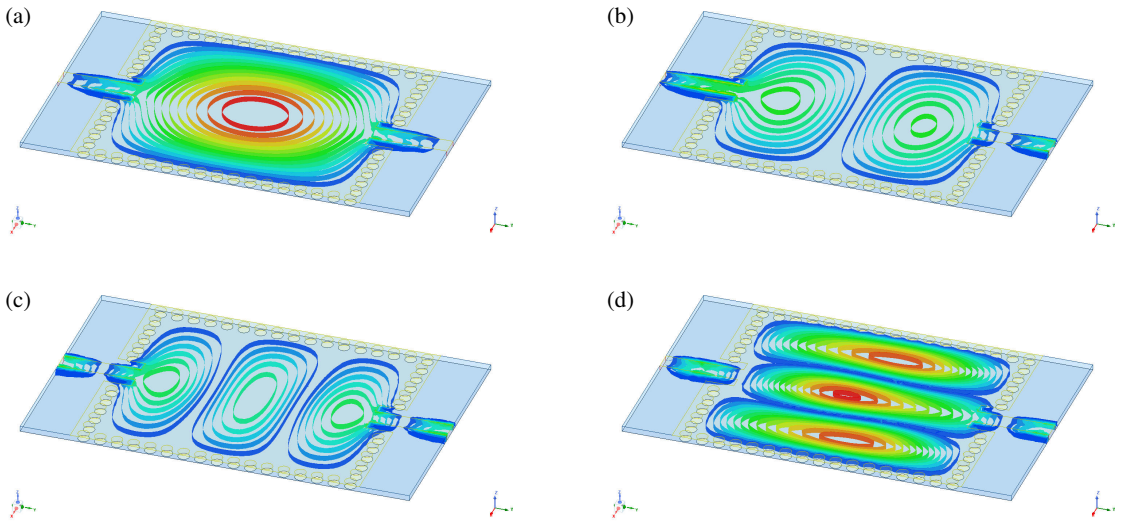

FIGURE 5. E-field distribution of the designed SIW cavity at different frequencies. (a) 3.25 GHz; (b) 4.8 GHz; (c) 6.72 GHz; (d) 7.88 GHz.

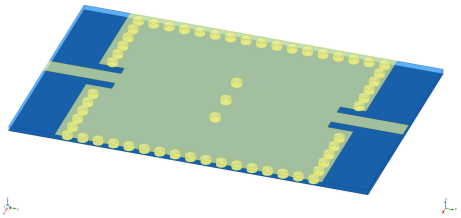

FIGURE 6. Structure of BPF_1.

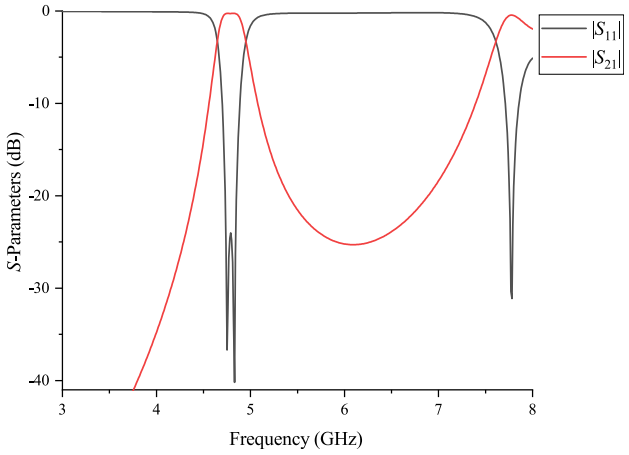

FIGURE 7. Simulated S-parameter of BPF_1.

plane. The geometrical structure of DGS typically makes it equivalent to a parallel LC circuit, which implies that it possesses stopband characteristics and can be utilized to introduce a transmission zero at specific frequencies to suppress the parasitic passband and enhance the stopband rejection. The DGS proposed in this design is a combination of dumbbell structure and Complementary Split Ring Resonator (CSRR), whose layout is depicted in Fig. 2(b). CSRR prolongs the current flow path by etching two open resonant rings with opposite openings on the ground plane, thereby increasing the equivalent inductance and equivalent capacitance. Furthermore, in comparison with spiral DGS, the geometric parameters of the CSRR structure are more adjustable, facilitating the attainment of transmission zero at a specific frequency and thereby enhancing the selectivity of the filter.

For a typical CSRR structure, as depicted in Fig. 9, the excitation from the vertical axial direction causes it to behave like a pair of electric dipoles. Hence, the CSRR can be regarded as a parallel LC circuit and can be utilized to generate a transmission zero. The self capacitance C_r and mutual inductance L_r of CSRR are given by

$$C_r = (4l_o - g_o)\, C_{out} + (4l_i - g_i)\, C_{in} \tag{5}$$

$$L_r = (4l_o - g_o)\, L_{out} + (4l_i - g_i)\, L_{in} \tag{6}$$

where C_{out} and L_{out} are the unit capacitance and unit inductance of the outer ring, while C_{in} and L_{in} are the corresponding parameters of the inner ring. From the above parameters, the resonant frequency of CSRR, i.e., the frequency point of the transmission zero, can be obtained as

$$f_{\text{CSRR}} = \frac{1}{2\pi\sqrt{L_r C_r}} \tag{7}$$

The equivalent circuit model of the proposed filter is depicted in Fig. 10. The two transmission modes in the SIW cavity respectively correspond to the ground parallel RLC circuit, both of which have band-pass characteristics. The DGS on the ground plane can be equivalent to an RLC parallel resonant circuit, which functions as band-stop.

4. RESULTS & DISCUSSIONS

4.1. Filter EM Simuation Result & Analysis

The simulated S-parameters of the proposed filter (referred to as BPF_2 hereinafter) with a variation of parameter W_d are shown in Fig. 11. It can be observed from Fig. 11 that the designed DGS generates a transmission zero near 7.2 GHz, successfully

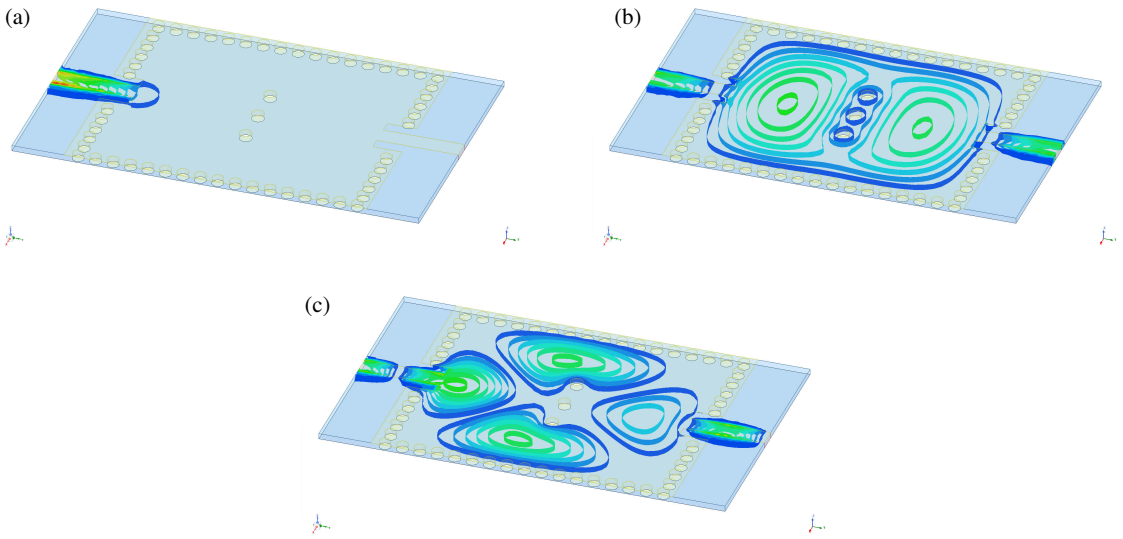

FIGURE 8. E-field distribution of BPF_1 at different frequencies. (a) 2.4 GHz; (b) 4.8 GHz; (c) 7.78 GHz.

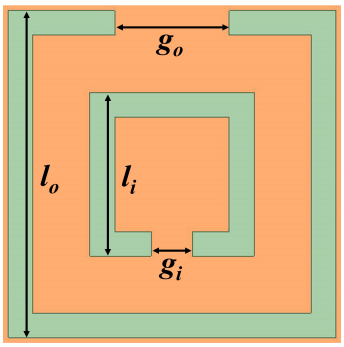

FIGURE 9. Typical CSRR structure.

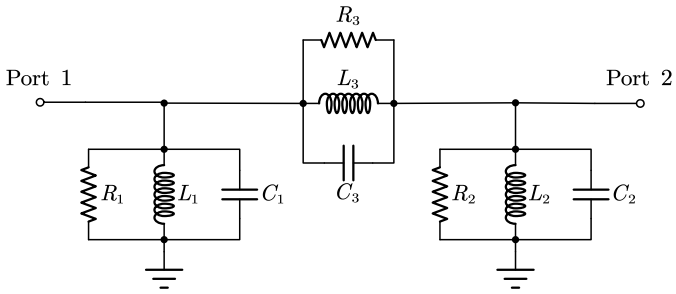

FIGURE 10. The equivalent circuit model of the proposed filter.

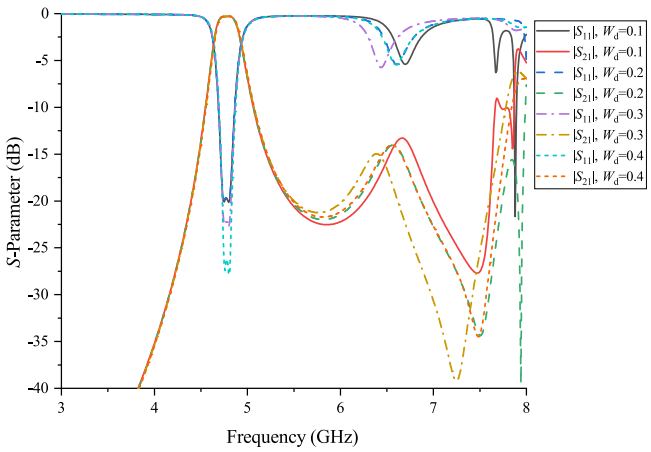

FIGURE 11. Effect of parameter W_d to the S-parameter of BPF_2.

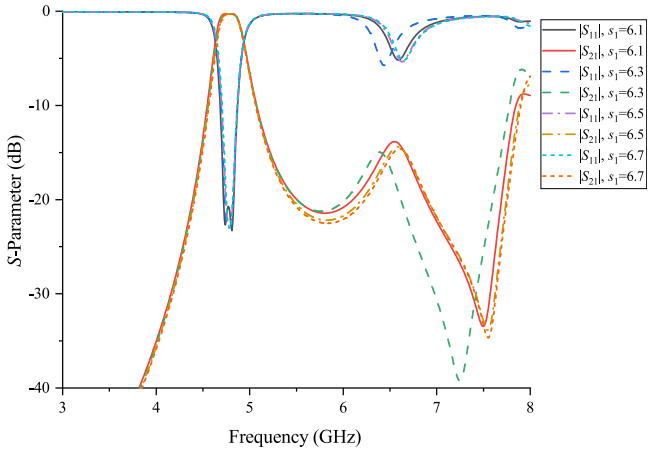

FIGURE 12. Effect of parameter s_1 to the S-parameter of BPF_2.

suppressing the parasitic passband of BPF_1. The return loss of BPF_2 in the passband deteriorates from 24.02 dB to 22.25 dB, which is attributed to the EM energy leakage caused by DGS. The left side of the passband of BPF_2 possesses excellent out-of-band attenuation, which can effectively suppress the interference caused by leaked fundamental waves.

As parameter W_d increases from 0.1 mm to 0.3 mm, the transmission zero introduced by DGS decreases from 7.48 GHz to 7.25 GHz, and the forward transmission coefficient dB($|S_{21}|$) at the transmission zero decreases from -27.7 dB to -39.2 dB, as the variation of parameter W_d modifies the equivalent capacitance and equivalent inductance

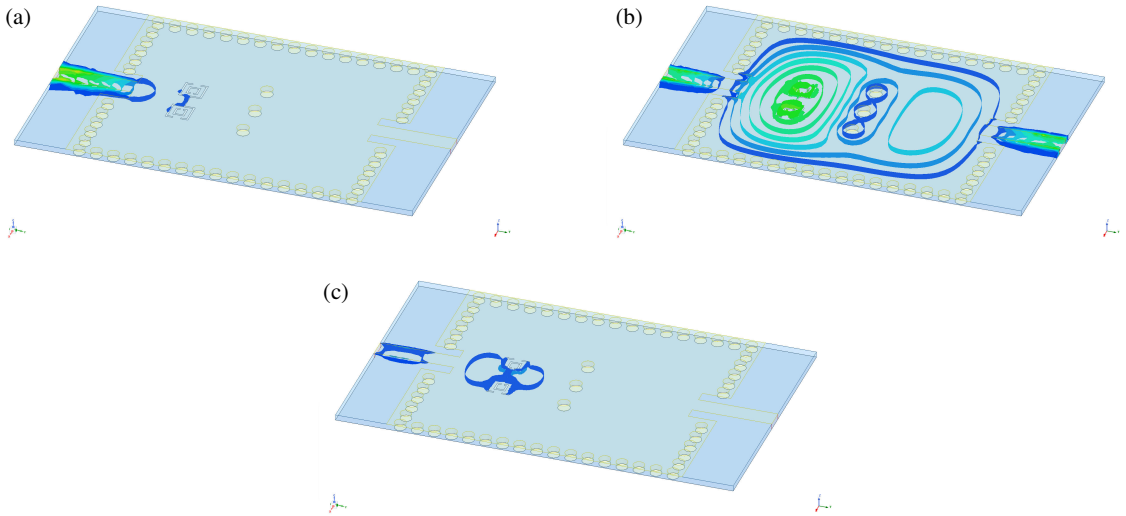

FIGURE 13. E-field distribution of BPF_2 at different frequencies. (a) 2.4 GHz; (b) 4.8 GHz; (c) 7.2 GHz.

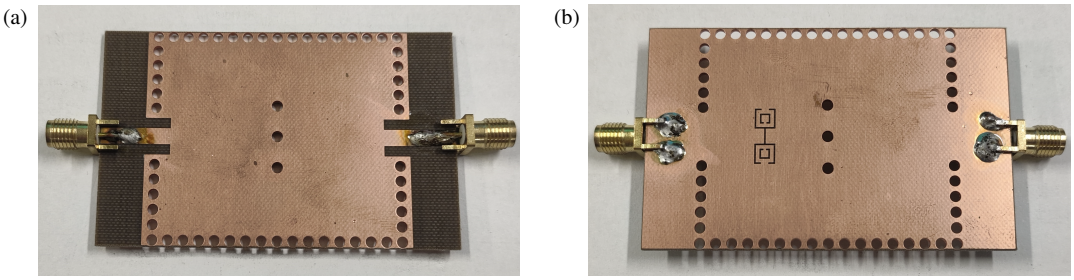

FIGURE 14. The physical filter. (a) Top side; (b) Bottom side.

of the designed DGS. However, as W_d continues to increase, the performance of dB($|S_{21}|$) at the transmission zero begins to deteriorate. Considering the above factors and the requirements to suppress the third harmonic transmission and parasitic passband in the designed filter, the value of parameter W_d is set at 0.3 mm.

The simulated S-parameter with a variation of parameter s_1 is presented in Fig. 12. It can be observed that with the increase of s_1, the resonant frequency of TE_{110} mode approaches that of TE_{120} mode, and the transmission poles in the passband change from two to one, which indicates that the degeneration occurs between these two resonant modes in the filter. Simultaneously, the 3 dB-bandwidth of the passband starts to shrink as s_1 increases. Additionally, the transmission zero generated by DGS is affected by the difference of s_1. Considering the above factors and design expectations, the parameter is set as $s_1 = 6.3$ mm.

The E-field distribution of BPF_2 at different frequencies is shown in Fig. 13. It can be observed that at the center frequency, the EM wave can pass through the filter smoothly, not affected by DGS. At the low-frequency stopband, the EM wave is basically reflected back to the input port due to the impedance mismatch. The high-frequency wave is blocked by DGS and thus cannot pass through the filter. These E-field diagrams are in line with the simulated S-parameter plot of the designed filter.

4.2. Comparison of Simulation & Measurement Results

The physical filter, as shown in Fig. 14, is fabricated by using PCB technology based on the optimized geometrical parameters from Table 1. During the test, it is necessary to solder the SMA-KHD connectors to the input and output ports of the physical filter, and then connect it to the Vector Network Analyzer (VNA) for measurement. The physical filter is connected to Deviser NA7682B VNA for measurement, and the EM simulation and VNA measurement results are both shown in Fig. 15. It can be observed from Fig. 15 that the overall S-parameter curve trends of the simulation and measurement are consistent. The measurement results show that the center frequency of the designed filter is 4.8 GHz; the 3 dB-bandwidth is 300 MHz; the insertion loss in the passband is approximately 0.5 dB; and the return loss in the passband is greater than 20 dB. Compared with the simulation result, the measured insertion loss is 0.2 dB greater; the measured return loss is 2.25 dB less than that of the simulation; and the designed transmission zero is shifted to the right in the frequency domain. The differences between the simulated and measured results are mainly attributed to the fabrication error, dielectric loss, and the inherent error of the VNA.

TABLE 2. Comparison with similar filters in the references.

Literatures	IL (dB)	RL (dB)	f_0 (GHz)	$BW_{3\,dB}$ (MHz)	Parasitic passband distance
[16]	2.47	11	3.9	520	near
[17]	1.02	19	4.0	640	near
[18]	0.92	21	15	570	near
[19]	0.9	17	7.5	390	far
[21]	1.9	18	26.6	5650	far
This work	0.5	20	4.8	300	far

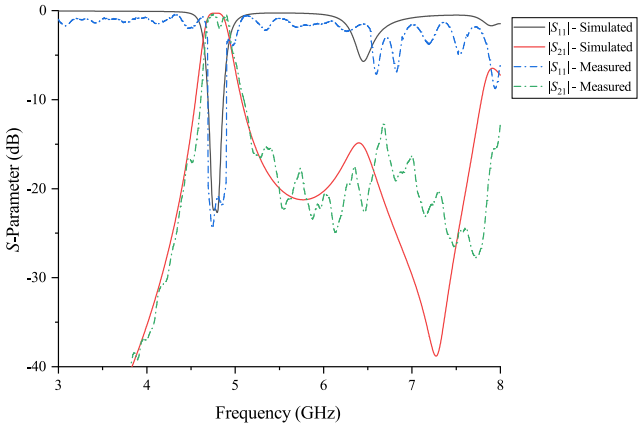

FIGURE 15. Simulated and measured S-parameters of designed filter.

A comparison of the performance of the designed filter with similar works in the referenced articles is presented in Table 2. The parasitic passband distance in the table refers to the distance between the center frequency of the filter passband and that of the parasitic passband. It can be concluded from the table that the proposed filter in this paper has lower insertion loss, higher return loss in the passband, better stopband rejection, and better suppression of the parasitic passband.

5. CONCLUSION

In this paper, a band-pass filter utilizing a dual-mode SIW cavity resonator with a novel DGS is proposed. The SIW cavity resonator operates in TE_{110} and TE_{120} modes, and the electric field of TE_{110} is modified by arranging a series of metallized disturbance holes at the center of the SIW cavity, to shift its resonant frequency to that of TE_{120} and form a passband at 4.8 GHz with two transmission poles. The DGS etched on the ground plane adopts a combination of a dumbbell structure and a CSRR. This DGS generates a transmission zero at 7.2 GHz, effectively suppressing the parasitic passband and enhancing the filter selectivity while having no negative influence on passband performance. Its overall layout is simple and innovative. The simulated and measured results indicate that the center frequency of the designed filter is 4.8 GHz; the 3 dB-bandwidth is 300 MHz; the insertion loss in the passband is up to 0.5 dB; and the return loss is greater than 20 dB. This paper combines a SIW cavity with a novel DGS to design the filter, whose center frequency, 3 dB-bandwidth, and transmission zero can be easily adjusted by varying the size of SIW cavity and geometrical dimensions of DGS based on diverse requirements. This filter can be utilized in the receiver system of NLJD to receive the second harmonic reflected by the nonlinear nodes and block the remaining interference signals, which holds certain practical significance in RF engineering.

ACKNOWLEDGEMENT

This work was supported in part by the Anhui Province Higher Education Science Research Project 2022AH050070, in part by the National Natural Science Foundation of China under Grant 62371002.

REFERENCES

[1] Bozzi, M., A. Georgiadis, and K. Wu, "Review of substrate-integrated waveguide circuits and antennas," *IET Microwaves, Antennas & Propagation*, Vol. 5, No. 8, 909–920, 2011.

[2] Chen, X.-P. and K. Wu, "Substrate integrated waveguide filters: Design techniques and structure innovations," *IEEE Microwave Magazine*, Vol. 15, No. 6, 121–133, 2014.

[3] Nwajana, A. O. and E. R. Obi, "A review on SIW and its applications to microwave components," *Electronics*, Vol. 11, No. 7, 1160, 2022.

[4] Jin, C. and Z. Shen, "Compact triple-mode filter based on quarter-mode substrate integrated waveguide," *IEEE Transactions on Microwave Theory and Techniques*, Vol. 62, No. 1, 37–45, 2014.

[5] Yang, X.-L., X.-W. Zhu, and X. Wang, "Dual-band substrate integrated waveguide filters based on multi-mode resonator overlapping mode control," *IEEE Transactions on Circuits and Systems II: Express Briefs*, Vol. 70, No. 6, 1971–1975, 2023.

[6] Chu, P., W. Hong, M. Tuo, K.-L. Zheng, W.-W. Yang, F. Xu, and K. Wu, "Dual-mode substrate integrated waveguide filter with flexible response," *IEEE Transactions on Microwave Theory and Techniques*, Vol. 65, No. 3, 824–830, 2017.

[7] Qiu, L.-F., L.-S. Wu, B. Xie, W.-Y. Yin, and J.-F. Mao, "Substrate integrated waveguide filter with flat passband based on complex couplings," *IEEE Microwave and Wireless Components Letters*, Vol. 28, No. 6, 494–496, 2018.

[8] Khandelwal, M. K., B. K. Kanaujia, and S. Kumar, "Defected ground structure: Fundamentals, analysis, and applications in modern wireless trends," *International Journal of Antennas and*

Propagation, Vol. 2017, No. 1, 2018527, 2017.

[9] Xu, S., K. Ma, F. Meng, and K. S. Yeo, "Novel defected ground structure and two-side loading scheme for miniaturized dual-band SIW bandpass filter designs," *IEEE Microwave and Wireless Components Letters*, Vol. 25, No. 4, 217–219, 2015.

[10] Kumar, C. and D. Guha, "Reduction in cross-polarized radiation of microstrip patches using geometry-independent resonant-type defected ground structure (DGS)," *IEEE Transactions on Antennas and Propagation*, Vol. 63, No. 6, 2767–2772, 2015.

[11] Wei, K., J.-Y. Li, L. Wang, Z.-J. Xing, and R. Xu, "Mutual coupling reduction by novel fractal defected ground structure bandgap filter," *IEEE Transactions on Antennas and Propagation*, Vol. 64, No. 10, 4328–4335, 2016.

[12] Chen, T., W. Tang, J. Mu, and T. J. Cui, "Microwave metamaterials," *Annalen Der Physik*, Vol. 531, No. 8, 1800445, 2019.

[13] Xu, H., Y. Wang, F. A. Ghaffar, and L. Roy, "Reconfigurable microwave filters implemented using field programmable microwave substrate," *IEEE Transactions on Microwave Theory and Techniques*, Vol. 69, No. 2, 1344–1354, 2021.

[14] Yang, C., C.-M. Guo, J. Xu, and H.-F. Zhang, "Device design for multitask graphene electromagnetic detection based on second harmonic generation," *IEEE Transactions on Microwave Theory and Techniques*, Vol. 72, No. 7, 4174–4182, 2024.

[15] Yang, C., C.-M. Guo, Y.-X. Wei, and H.-F. Zhang, "Electromagnetic detection design in liquid crystals janus metastructures based on second harmonic generation," *IEEE Transactions on Instrumentation and Measurement*, Vol. 73, 1–11, 2024.

[16] Tomassoni, C., L. Silvestri, M. Bozzi, and L. Perregrini, "Substrate-integrated waveguide filters based on mushroom-shaped resonators," *International Journal of Microwave and Wireless Technologies*, Vol. 8, No. 4-5, 741–749, 2016.

[17] Moscato, S., C. Tomassoni, M. Bozzi, and L. Perregrini, "Quarter-mode cavity filters in substrate integrated waveguide technology," *IEEE Transactions on Microwave Theory and Techniques*, Vol. 64, No. 8, 2538–2547, 2016.

[18] Chu, P., W. Hong, M. Tuo, K.-L. Zheng, W.-W. Yang, F. Xu, and K. Wu, "In-line ports dual-mode substrate integrated waveguide filter with flexible responses," *IEEE Microwave and Wireless Components Letters*, Vol. 28, No. 10, 882–884, 2018.

[19] Chu, P., P. Zhu, J. Feng, L. Guo, L. Zhang, F. Zhu, L. Liu, G. Q. Luo, and K. Wu, "Substrate integrated waveguide filter with flexible mixed coupling," *IEEE Transactions on Microwave Theory and Techniques*, Vol. 71, No. 9, 4003–4011, 2023.

[20] Mazzaro, G. J., "Nonlinear junction detection vs. electronics: System design and improved linearity," in *2020 IEEE International Radar Conference (RADAR)*, 654–658, Washington, DC, USA, 2020.

[21] Li, J., W. Zheng, X. Wei, Y. Huang, and G. Wen, "Millimeter-wave substrate integrated waveguide bandpass filters based on stepped-impedance E-shaped defected ground structures," *International Journal of RF and Microwave Computer-Aided Engineering*, Vol. 32, No. 11, e23340, 2022.